Scanning tunneling microscopy studies of gold(111) derivatized with organothiols

Yeon Taik Kim, Robin L. McCarley, and Allen J. Bard

J. Phys. Chem., **1992**, 96 (18), 7416-7421 • DOI: 10.1021/j100197a052

(5) Gao, X.; Hamelin, A.; Weaver, M. J. *Phys. Rev. Lett.* **1991**, *67*, 618.
(6) Hillner, P. E.; Gratz, A. J.; Manne, S.; Hansma, P. K. Submitted to *Geology*.
(7) Chang, H.; Bard, A. J. *J. Am. Chem. Soc.* **1991**, *113*, 5588.
(8) Binnig, G.; Rohrer, H. *IBM J. Res. Dev.* **1986**, *30*, 355.
(9) Cataldi, T. R. I.; Blackman, I. G.; Briggs, G. A. D.; Pethica, J. D.; Hill, H. A. O. *J. Electroanal. Chem.* **1990**, *290*, 1.
(10) Yau, S.-L.; Vitus, C. M.; Schardt, B. C. *J. Am. Chem. Soc.* **1990**, *112*, 3677.
(11) Nagahara, L. G.; Thundat, T.; Oden, P. I.; Lindsay, S. M.; Rill, R. L. *Ultramicroscopy* **1990**, *33*, 107.
(12) Chidsey, C. E. D.; Loaicono, D. N.; Sleator, T.; Nakahara, S. *Surf. Sci.* **1988**, *200*, 45.
(13) Hallmark, V. M.; Chiang, S.; Rabolt, J. F.; Swalen, J. D.; Wilson, R. J. *Phys. Rev. Lett.* **1987**, *59*, 2879.
(14) Widrig, C. A.; Alves, C. A.; Porter, M. D. *J. Am. Chem. Soc.* **1991**, *113*, 2805.
(15) McCarley, R. L.; Bard, A. J. *J. Phys. Chem.* **1991**, *95*, 9618.
(16) Hashimoto, S.; Miura, S.; Kubo, T. *J. Mater. Sci.* **1976**, *11*, 1501.
(17) Oppenheim, I. C.; Trevor, D. J.; Chidsey, C. E. D.; Trevor, P. L.; Sieradski, K. *Science* **1991**, *254*, 687.
(18) Kirk, D. W.; Foulkes, F. R. *J. Electrochem. Soc.* **1980**, *127*, 1993.
(19) Kunimatsu, K.; Seki, H.; Gorgon, W. G.; Philpott, M. R. *Langmuir* **1988**, *4*, 337.
(20) Wadsworth, M. E. *Min. Eng. (Littleton, Colo.)* **1985**, *37*, 557.
(21) Kudryk, K. V.; Kellogg, H. H. *J. Met.* **1954**, *6*, 541.
(22) Trevor, D. J.; Chidsey, C. E. D. *J. Vac. Sci. Technol., B* **1991**, *9*, 964.
(23) Michely, T.; Besocke, K. H.; Comsa, G. *Surf. Sci. Lett.* **1990**, *230*, L135.
(24) Jaklevic, R. C.; Elie, L. *Phys. Rev. Lett.* **1988**, *60*, 120.
(25) Sette, F.; Hashizume, T.; Comin, F.; MacDowell, A. A.; Citrin, P. H. *Phys. Rev. Lett.* **1988**, *61*, 1384.
(26) Trevor, D. J.; Chidsey, C. E. D.; Loiacono, D. N. *Phys. Rev. Lett.* **1989**, *62*, 929.

Scanning Tunneling Microscopy Studies of Au(111) Derivatized with Organothiols

Yeon-Taik Kim, Robin L. McCarley, and Allen J. Bard*

Department of Chemistry and Biochemistry, The University of Texas at Austin, Austin, Texas 78712
(Received: February 20, 1992; In Final Form: April 28, 1992)

Atomic resolution scanning tunneling microscopy (STM) images of various-sized organothiols adsorbed on Au(111) display a $(\sqrt{3} \times \sqrt{3})R30°$ structure, even when the ω-substituent size (4.3–13 Å) is so large that such a packing should not be possible. The observation of a $(\sqrt{3} \times \sqrt{3})R30°$ structure for thiols that should pack less densely suggests that the observed images are of gold electronic distributions that have been perturbed by the adsorbed thiol.

Introduction

We report here atomic resolution scanning tunneling microscopy images of the Au(111) surface derivatized with various-sized organothiols (4-aminothiophenol, $[Ru(bipyridine)_2(4\text{-methyl-}4'\text{-}(12\text{-mercaptododecyl})\text{-}2,2'\text{-bipyridine})](PF_6)_2$, $(C_5H_5)Fe(C_5H_4CO_2(CH_2)_{16}SH)$, [2]staffane-3,3′-dithiol pentaammineruthenium(II) hexafluorophosphate, and [2]staffane-3,3′-dithiol silver Figure 1) via self-assembly. The surface showed $(\sqrt{3} \times \sqrt{3})R30°$ superlattice structures regardless of the physical size of the substituent group of the thiol. The physical size of the ω-substituent varied from 4.3 to 13 Å. The unexpected $(\sqrt{3} \times \sqrt{3})R30°$ structure, especially in cases where such a packing was prevented by the size of the ω-substituent, is interpreted as electronic in nature and is caused by a spatial extension of Au wave functions on neighboring sites induced by the adsorbed species on the Au surface.

Following the invention of the scanning tunneling microscope (STM),[1] remarkable atomic and molecular structures have been elucidated in different environments such as air, liquid, and ultrahigh vacuum.[2] Recently, STM has been used to study the topography of organic monolayers formed by the Langmuir–Blodgett technique or self-assembly.[3] Because the STM is blind to the actual chemical nature of the adsorbed species and only responds to electron density, the images obtained can be easily misinterpreted while attempting to understand real topographic features. For example, images of the basal plane of highly oriented pyrolytic graphite (HOPG) obtained with the STM only show every other carbon atom because of an asymmetric electron density between adjacent carbon atom sites.[4] This difference in sites is intrinsic to graphite (0001) which has an AB stacking sequence. Moreover, another STM study of graphite showed long range electronic perturbations caused by defects or adsorbates.[5] The defects or adsorbates perturb the charge density resulting in an anomalous $(\sqrt{3} \times \sqrt{3})R30°$ superlattice structure. Such superlattice structures on HOPG were interpreted as a change in the electronic structure of carbon atoms rather than a lattice reconstruction. Furthermore, STM studies have yielded images of graphite with a large scale hexagonal pattern with spacings varying from 4 to 110 Å, depending on the experimental conditions.[6] Charge density waves observed by STM with low dimensional materials are another example of electronic structures caused by a slight displacement of the atoms.[7] In this paper we suggest that the $(\sqrt{3} \times \sqrt{3})R30°$ structure on Au(111)/mica derivatized with a monolayer of organothiols is the result of Au electronic perturbations, rather than actual imaging of the monolayer itself.

Experimental Section

Chemicals. The 4-aminothiophenol (4-ATP) was purchased from Aldrich and vacuum-sublimed prior to use. Staffane compounds ([2]staffane-3,3′-dithiol ([2]S-dithiol), [2]staffane-3,3′-dithiol pentaammineruthenium(II) hexafluorophosphate (Ru-[2]-S-dithiol) were obtained from Professor Josef Michl, and detailed synthetic methods for these compounds are described elsewhere.[8] The $[Ru(bpy)_2(4\text{-methyl-}4'\text{-}(12\text{-mercaptododecyl})\text{-}2,2'\text{-bipyridine})](PF_6)_2$, abbreviated as Rub_2b^*, and $(C_5H_5)Fe(C_5H_4CO_2(CH_2)_{16}SH)$ were provided by Drs. Y. S. Obeng and D. Collard, respectively. Synthetic methods for these thiols can be found in the literature.[9,10] $AgNO_3$ (99.9999%) was obtained from Aldrich and used to make the staffane dithiol–Ag complex. Absolute ethanol and HPLC grade acetone were used without further purification. All other chemicals were reagent grade or better.

Substrate Preparation and Monolayer Formation. Approximately 150 nm thick Au(111) films were evaporated onto mica substrates as previously described.[11] Briefly, Au(111) films were prepared by thermal evaporation of high-purity Au (99.99%) at 0.2 nm s^{-1} onto heated mica in a Plasmatron P-30 thin film system operating at 2×10^{-6} Torr vacuum. The mica (Asheville-Schoonmaker, Newport News, VA) was heated to 310 °C and held there for 30 min before deposition was carried out. Once the substrates had cooled to near 100 °C, the chamber was back-filled with nitrogen and the Au/mica films were placed in ethanol (0.25 mM ferrocene thiol, 10 mM 4-ATP, 0.1 mM [2]-S-dithiol, and 0.1 mM Ru-[2]S-dithiol) or acetone (0.25 mM

0022-3654/92/2096-7416$03.00/0

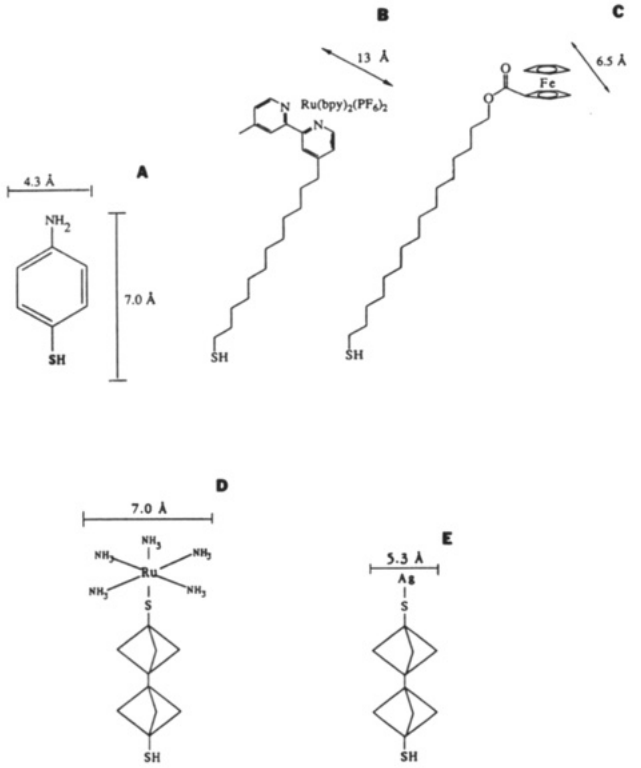

Figure 1. Structures of organothiols used: A, 4-aminothiophenol (4-ATP); B, $[Ru(bpy)_2(4\text{-methyl-}4'\text{-}(12\text{-mercaptododecyl})\text{-}2,2'\text{-bipyridine})](PF_6)_2$ (abbreviated as Rub_2b^*); C, $(C_5H_5)Fe(C_5H_4CO_2(CH_2)_{16}SH)$; D, Ru–[2]S-dithiol; E, [2]S-dithiol–Ag.

ruthenium thiol) solutions of the thiols for approximately 24 h at room temperature to form monolayers known in the literature.[12] The Au(111)/mica substrates were removed from the thiol solutions, rinsed with copious amounts of appropriate solvent, dried with nitrogen gas, and then transferred to the STM for imaging. The [2]S-dithiol–Ag complex was formed by immersing the Au(111)/mica in 0.1 mM [2]S-dithiol solution in absolute EtOH resulting in a monolayer of [2]S-dithiol on Au(111)/mica. The modified substrate was then exposed to 1 mM $AgNO_3$ aqueous solution for 5 min, washed with distilled water (18 MΩ cm), and dried in a N_2 stream.

Instrumentation. Images were obtained with a NanoScope II scanning tunneling microscope (Digital Instruments, Santa Barbara, CA) using mechanically cut (GC Electronics diagonal cutters) Pt/Ir (80:20) tips. All experiments were performed with the specimen in air. STM images were obtained in the constant-height mode with a fast data acquisition rate (19–78 Hz per line, 400 × 400 data points). The tunneling parameters were varied with a bias (V_b) of ±5 to ±300 mV and a tip current (I_t) of 0.2–20 nA.

Results and Discussion

Atomic Images of Freshly Prepared Au(111). A typical STM image of an evaporated Au(111) film on mica is shown in Figure 2. The atomic spacing of the hexagonally close packed surface was found to be 2.9 ± 0.3 Å, in good agreement with literature values for the Au(111) surface.[13] The atomic image was reproducibly observed with a number of freshly prepared Au samples using various tunneling parameters, i.e., V_b = 5–100 mV, I_t = 1–10 nA. We did not observe any other spacings except the hexagonal spacing shown in Figure 1.

Atomic Images of Au(111)/Mica Derivatized with 4-ATP. Figure 3A is an STM image of a 4-ATP modified Au(111) surface. It shows a nearest spacing of 4.9 ± 0.3 Å and a next-nearest neighbor spacing of 8.9 ± 0.5 Å. This spacing is consistent with a $(\sqrt{3} \times \sqrt{3})R30°$ structure and a maximum coverage, Θ, of $^1/_3$. The two-dimensional Fourier spectrum of the raw data is also shown in Figure 3B. Only one set of hexagonal dots is seen, indicating that the $(\sqrt{3} \times \sqrt{3})R30°$ structure is the only discernible structure after the adsorption of the 4-ATP. Thus the STM image in Figure 3A is consistent with a true adlattice structure of 4-ATP. This can be further justified by the following. First, electrochemical oxidation of the surface bound 4-ATP in 0.1 M H_2SO_4 provided the macroscopic quantification of the adsorbed species. The integrated charge under the oxidation peak of the cyclic voltammogram corresponding to the oxidation of the aniline moiety (not shown) revealed a coverage of 0.23–0.30 depending on roughness factor assumed (1.0–1.5); this agrees well with the maximum surface coverage obtained by STM (0.33). Second, the physical dimensions of the 4-ATP molecule, shown in Figure 1A, are small enough to allow a $(\sqrt{3} \times \sqrt{3})R30°$ packing structure on Au(111). These results are in agreement with recent STM reports concerning the adlayer structure of alkanethiol-covered Au(111) surfaces where the adlattice was reported to have the $(\sqrt{3} \times \sqrt{3})R30°$ structure.[3a]

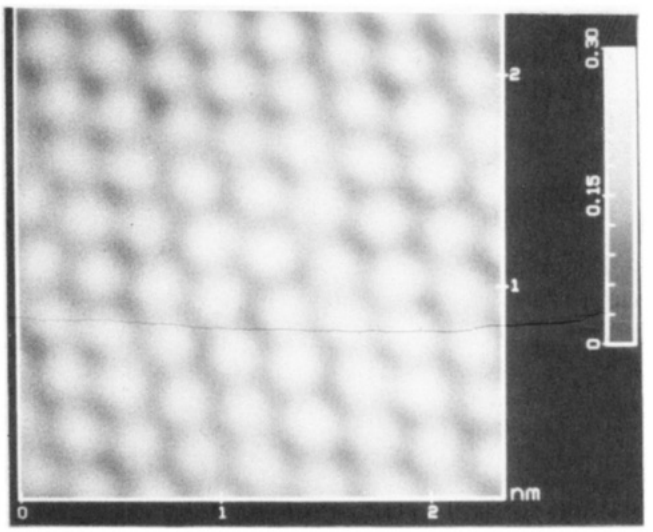

Figure 2. Spectrum-filtered STM image of a 23 Å × 23 Å region of bare Au(111)/mica film: constant-current mode; V_b = +4.9 mV; I_t = 3.0 nA.

STM Imaging of Rub_2b^*. Unfiltered, constant-height images of two areas on the same type of Au(111) surface modified with Rub_2b^* are displayed in parts A and B of Figure 4. Atomic features are clearly seen on the terraces, with these features being slightly less well-defined at the terrace step edges. These images were stable for over an hour, and similar images could be found practically everywhere on the sample. An enlarged view of Figure 4A is shown in Figure 4B. There appears to be only one spacing of atomic species as demonstrated by the two-dimensional Fourier spectrum of the image in Figure 4B, Figure 4D. Only one set of spots can be discerned, indicating that the data exhibit *one* characteristic frequency. The nearest and next-nearest neighbor spacings were found to be 5.1 ± 0.3 and 8.7 ± 0.5 Å. These data along with the two-dimensional Fourier spectrum information indicate that the image is characteristic of a $(\sqrt{3} \times \sqrt{3})R30°$ structure. No other spacing was observed on a number of samples examined, nor was there any other pattern superimposed on top of the apparent $(\sqrt{3} \times \sqrt{3})R30°$ structure.

The physical dimensions of the Rub_2b^*, shown in Figure 1B, indicate that the large ω-substituent, namely the $Ru(bpy)_3^{2+}$, with a dimension of approximately 13 Å, would not allow a packing as close as the 5.1 Å shown in Figure 4A–C. Moreover, electrochemical surface coverage measurements based on the Ru(II/III) wave in acetonitrile media give values (Θ = 0.034–0.028) which are in good agreement with those predicted by a close packing model of spheres with a diameter of 13 Å (Θ = 0.04). One could argue that the Rub_2b^* might adopt a floppy organization on the surface, allowing for small regions of $(\sqrt{3} \times \sqrt{3})R30°$ structure, but this could not occur over the large domains shown in Figure 4A. The stability of these images, as well as the ability to obtain similar images on other areas of the sample, indicates that the tip does not degrade the sampled areas as a function of time. When the tunneling current was decreased, the

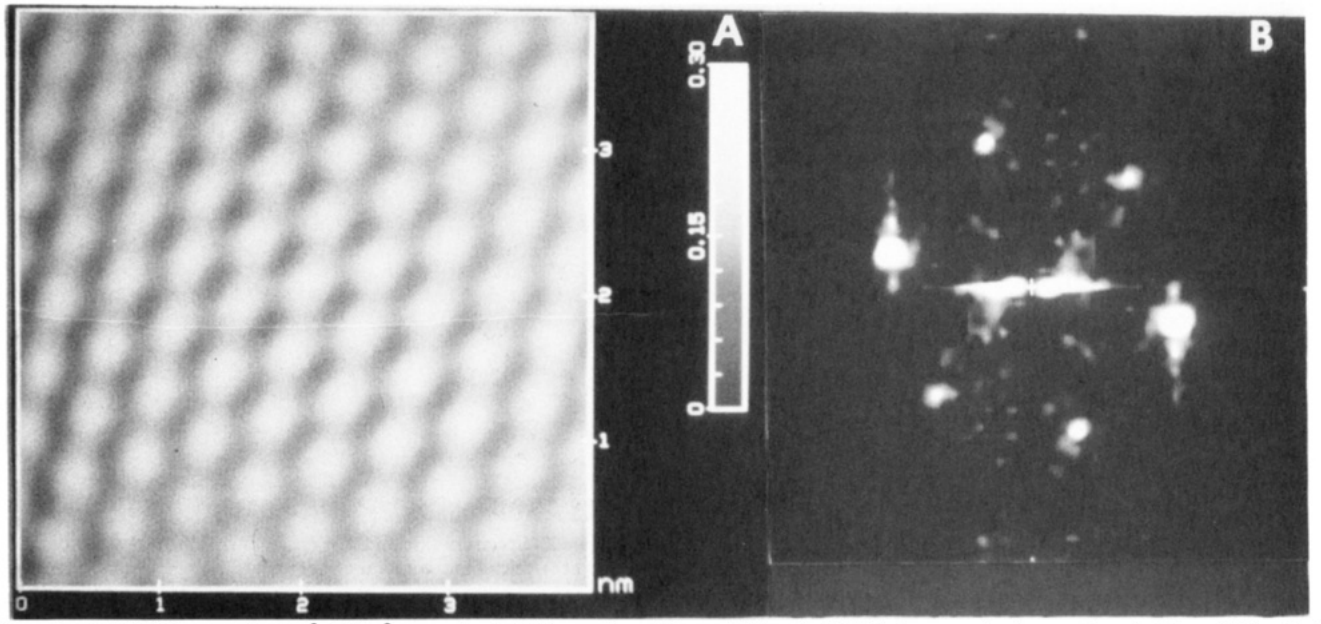

Figure 3. (A) STM image of a 40 Å × 40 Å area of a 4-ATP monolayer film coated on Au(111)/mica: constant-current mode; V_b = −31.1 mV; I_t = 6.2 nA. (B) Two-dimensional Fourier spectrum of raw data shown in A. The hexagonal pattern is used to construct the image shown in A.

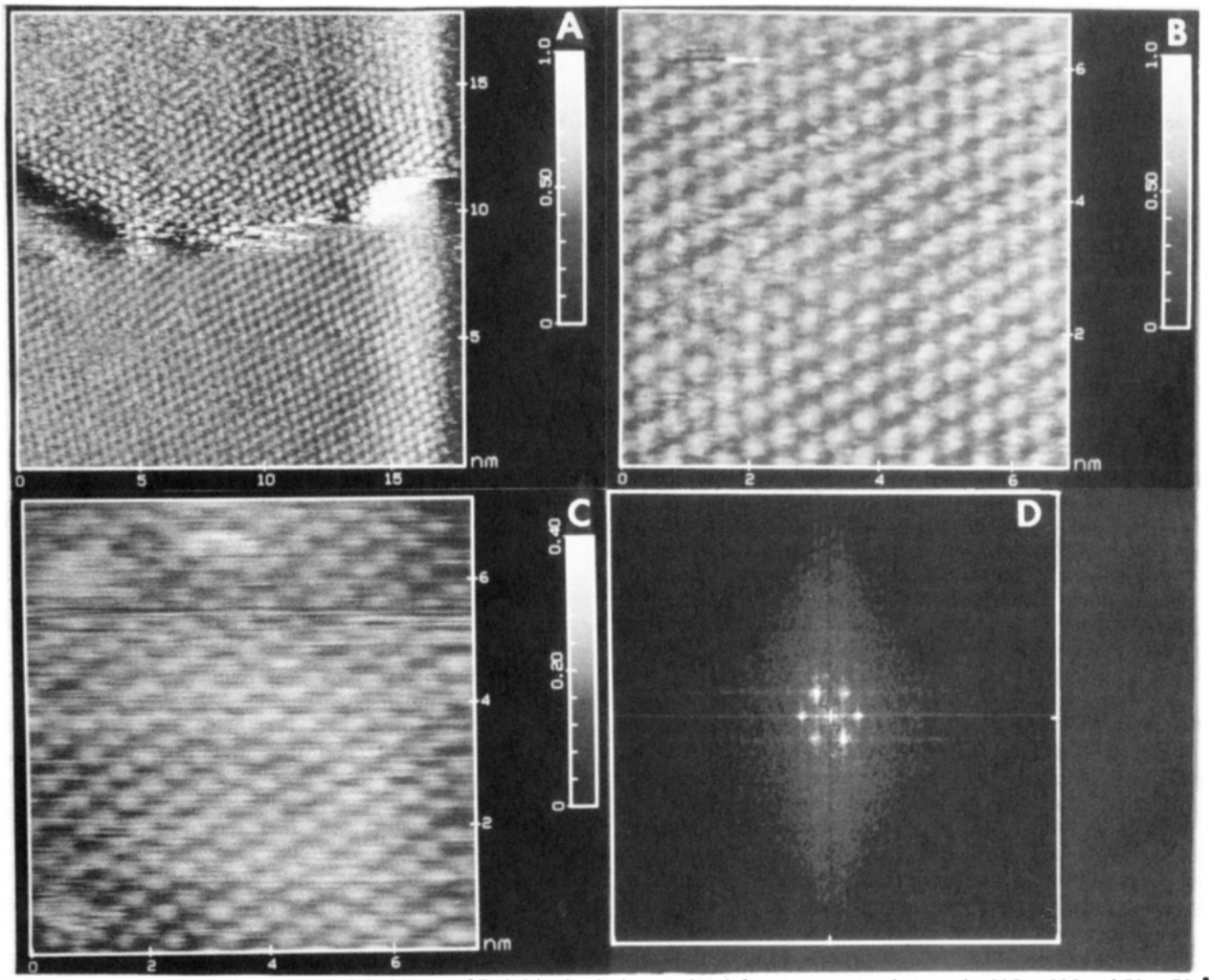

Figure 4. (A and B) Unfiltered, constant-height images of Rub_2b^* adsorbed on Au(111) for two areas on the sample, 225 × 225 and 70 × 70 Å for A and B, respectively. (C) Unfiltered, constant-current image of the area in B. I_t = 1 nA and V_b = 20 mV. (D) Two-dimensional Fourier spectrum of raw data in B.

image quality (resolution) was poorer, but again became better when the tunneling current was returned to its original value. No other spacings were observed. In addition, constant-current images exhibited only one atomic spacing, Figure 4C, identical to that obtained in the constant-height mode. The ability to image such large areas in both the constant-current and height modes along with the lack of a superimposed image variation on top of the $(\sqrt{3} \times \sqrt{3})R30°$ structure makes it difficult to explain how the ob-

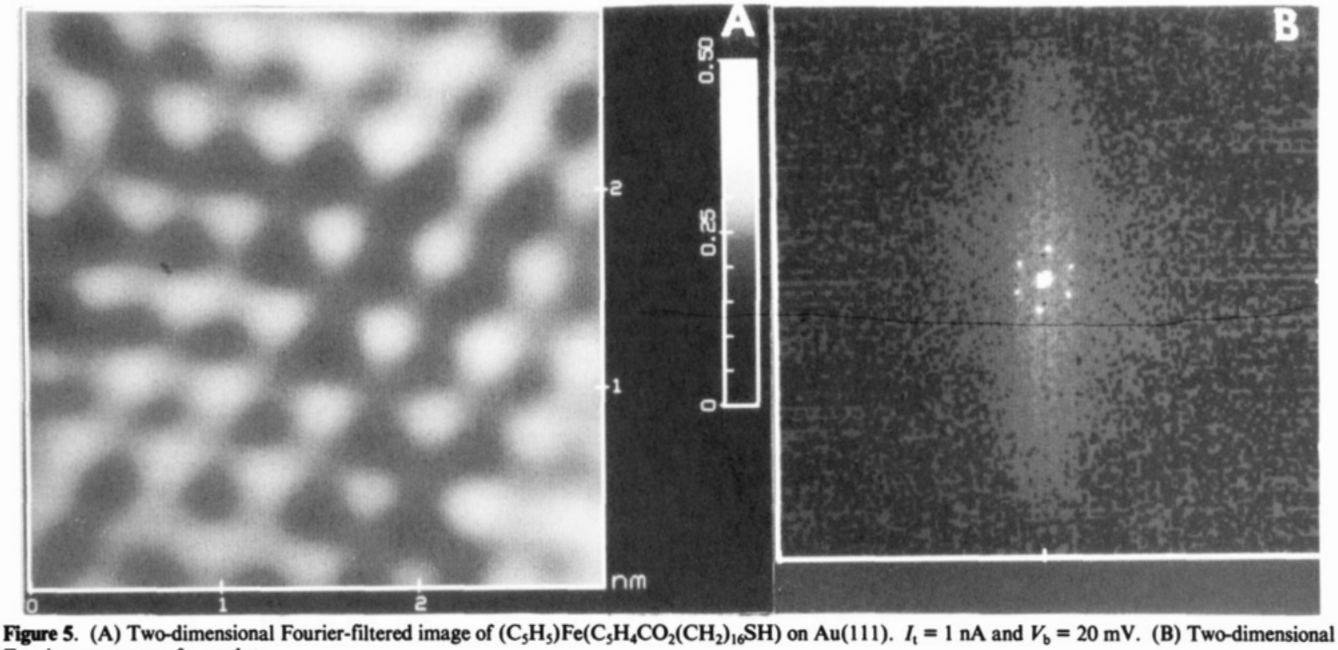

Figure 5. (A) Two-dimensional Fourier-filtered image of $(C_5H_5)Fe(C_5H_4CO_2(CH_2)_{16}SH)$ on Au(111). I_t = 1 nA and V_b = 20 mV. (B) Two-dimensional Fourier spectrum of raw data.

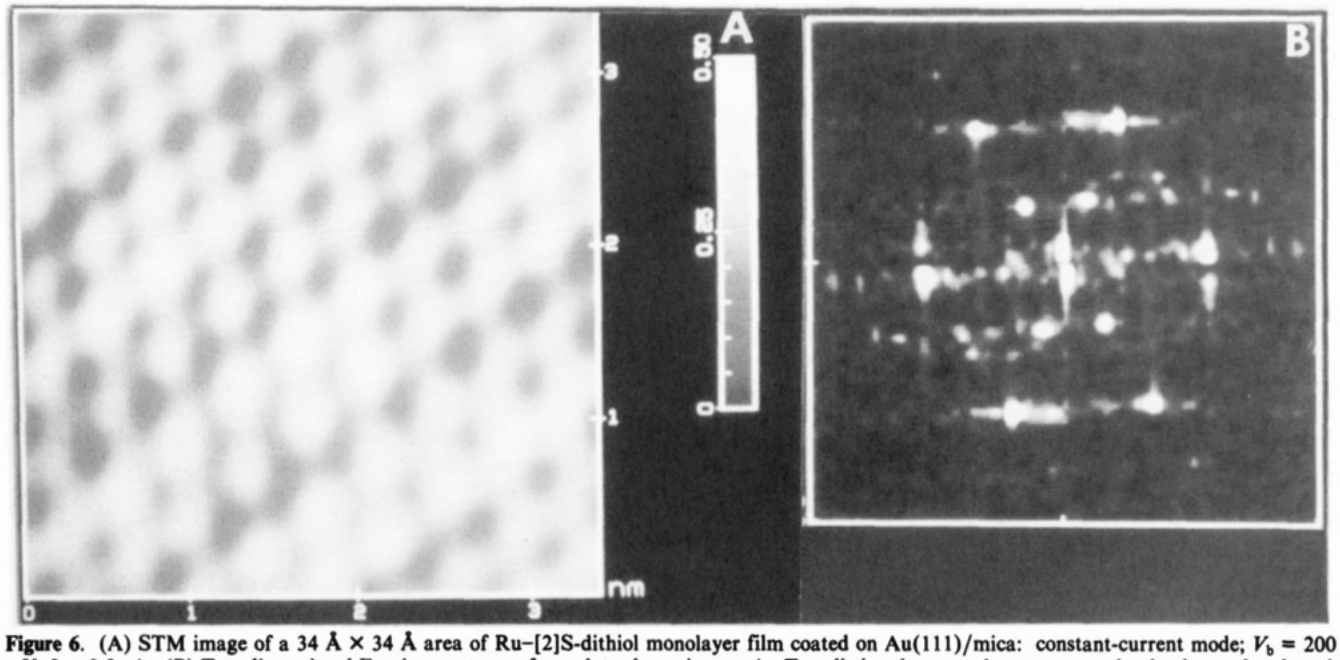

Figure 6. (A) STM image of a 34 Å × 34 Å area of Ru–[2]S-dithiol monolayer film coated on Au(111)/mica: constant-current mode; V_b = 200 mV; I_t = 0.5 nA. (B) Two-dimensional Fourier spectrum of raw data shown in part A. Two distinct hexagonal patterns are clearly observed and used to construct the image shown in part A.

tained image arises for the Rub_2b^*. An alternative explanation is that the surface electronic distribution is perturbed by the adsorbate on the Au(111). It is this distribution that is probed by the tip, and the electron density has a frequency equal to $\sqrt{3}$ times the Au spacing, as discussed in more detail below. As mentioned previously, an analogous result has been found with STM of adsorbates on HOPG.[5]

Images of $(C_5H_5)Fe(C_5H_4CO_2(CH_2)_{16}SH)$. To investigate a long chain alkanethiol with an ω-substituent smaller than that of the Rub_2b^*, the ferrocene-substituted thiol $(C_5H_5)Fe(C_5H_4CO_2(CH_2)_{16}SH)$ was used. The ferrocene group has a physical dimension of approximately 6.5 Å, Figure 1C, which is still much larger than the 5 Å nearest neighbor spacing expected for the $(\sqrt{3} \times \sqrt{3})R30°$ structure. Upon examination with STM, the ferrocenethiol-coated Au(111) samples exhibited atomic species with only one characteristic spacing, as demonstrated by Figure 5A and the two-dimensional Fourier spectrum of the STM image, Figure 5B. Nearest and next-nearest neighbor spacings of 5.2 ± 0.3 and 8.9 ± 0.5 Å were obtained, respectively, again pointing to a $(\sqrt{3} \times \sqrt{3})R30°$ adlayer. Once again the size of the substituent group is such that the monolayer cannot pack closer than the expected 6.5 Å, but the observed packing obtained from the STM image is 5 Å. Electrochemical surface coverage measurements based on the Fc/Fc^+ wave in 1.0 M $HClO_4$ (θ = 0.21–0.15) agree well with previous literature values[14] and those predicted by a close packed model (θ = 0.18), with a sphere diameter of 6.5 Å. Although it is difficult to explain quantitatively the origin of the image of the ferrocenethiol, we believe that again the image is really an electronic state of the gold induced by the adsorbed thiol.

Atomic Images of Au(111)/Mica Derivatized with Ru–[2]S-dithiol. Figure 6A is an STM image of a Ru–[2]S-dithiol modified Au(111) surface. The corresponding two-dimensional Fourier spectrum is shown Figure 6B. It clearly indicates two different sets of hexagonal periodicities on the surface. The outer hexagonal structure shows a nearest spacing of 4.8 ± 0.3 Å and a next nearest neighbor spacing of 8.7 ± 0.5 Å, again a $(\sqrt{3} \times \sqrt{3})R30°$ structure. Another set of spots (the inner hexagonal set) represents

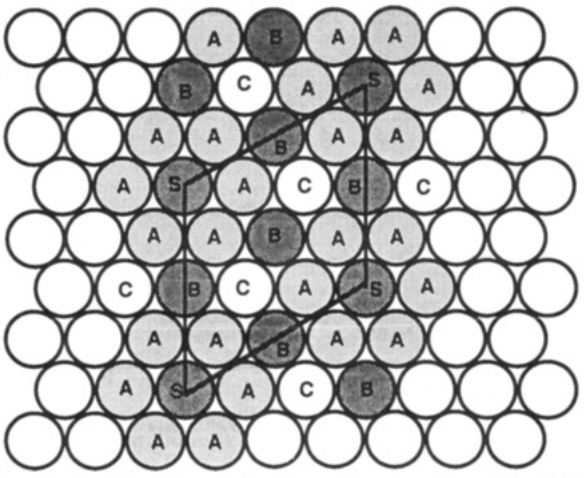

Figure 7. Possible different Au atoms after adsorption of Ru–[2]S-dithiol.

a nearest spacing of 9.8 ± 0.5 Å and a next-nearest neighbor spacing of 17.4 ± 1 Å, which corresponds to a $2(\sqrt{3} \times \sqrt{3})R30°$ structure. In addition, the two sets of hexagonal dots are in the same direction relative to the underlying Au(111) as seen in the two-dimensional Fourier spectrum. Thus it is clear that the frequency of the one hexagonal set of spots is exactly twice that of the other and the two frequencies are superimposed to form the STM image in Figure 6A. This image was reproducible for different batches of the sample.

To identify the cause of the atomic corrugation observed in Figure 6A, the physical size of a Ru–[2]S-dithiol molecule with respect to the underlying Au(111) was considered. The closest packing distance of the Ru–[2]S-dithiol should be determined by the size of the $Ru(NH_3)_5$ substituent. (Note that the diameter of the staffane cage is approximately 5.3 ± 0.2 Å[15] and that of $Ru(NH_3)_5$ is approximately 7.0 ± 0.2 Å[16] as shown in Figure 1D.) Thus the Ru–[2]S-dithiol cannot pack closer than 7.0 Å. A $2(\sqrt{3} \times \sqrt{3})R30°$ structure, which is represented by the inner set of spots in Figure 6A, is the only possible closest hexagonal packing arrangement, if the adsorption of Ru–[2]S-dithiol is commensurate with the underlying Au(111) by occupying identical sites (hcp *or* fcc) as marked by "S" on the Au(111) surface, Figure 7. With such a packing density, a maximum surface coverage, Θ, of $^1/_6$ can be achieved. When the macroscopic surface coverage was estimated by the electrochemical oxidation of the Ru(II) moiety of the surface-bound Ru–[2]S-dithiol, values of 0.151–0.202 (roughness factors of 1.5–2.0 were used for the sputtered Au electrode[8c]) were observed. These values are in good agreement with those determined from STM. On the basis of the above observation, we believe the periodicity of the $2(\sqrt{3} \times \sqrt{3})R30°$ structure can be explained as either a Ru–[2]S-dithiol STM image or a modified Au atom image induced by the adsorption of thiol compound.

Model for Observed $(\sqrt{3} \times \sqrt{3})R30°$ Pattern. The anomalous hexagonal $(\sqrt{3} \times \sqrt{3})R30°$ structure, which was observed for the above samples, cannot be explained by the actual packing of the Ru–[2]S-dithiol or ferrocene or Rub_2b^* compounds. We propose rather that the Au(111) atomic structure is modified by the adsorbate. The effect might be caused by the adsorption of Ru–[2]S-dithiol species on Au atoms leading to a perturbation of the wave functions on neighboring Au atoms. As seen in Figure 7, when the Ru–[2]S-dithiol is assumed to be adsorbed on "S" sites, the electronic structure of the surrounding six Au atoms (marked as "A") can be strongly influenced. This would cause an asymmetric electron density distribution among the other Au atoms, resulting in two different types of Au atoms, "B" and "C", which are surrounded by "AACAAC" or "ABABAB". The combined "S" and "B" images may then form the STM image shown in Figure 6A. The asymmetric electronic density of the substrate prevents the "A" and "C" atoms from being detected by STM and results in the $(\sqrt{3} \times \sqrt{3})R30°$ structure.

Although this argument is somewhat speculative, we feel it is the most plausible explanation of the images. The nature of the organosulfur/Au interaction has been shown to be covalent[3g,h] and should strongly alter the density of states at the "S" sites but have less of an effect on the sites away from the adsorption site. Because there is nothing in the literature concerning theoretical models of STM imaging of modified Au surfaces, we can only turn to that information regarding similar structures on HOPG.

It should be noted that atomic images were easier to obtain with Ru–[2]S-dithiol compared to pure [2]S-dithiol adsorbed on the Au(111)/mica, although the $Ru(NH_3)_5$ group made the monolayers thicker. The role of the metallic group seems to be important to achieve such atomic images. This will be discussed further in the next section.

Atomic Images of Au(111)/Mica Surface Derivatized with a [2]S-dithiol–Ag. The effect of a metal (Ag) on the STM image of a staffanedithiol was also investigated. Figure 8A shows an STM image of Au(111) after the adsorption of [2]S-dithiol–Ag. Many attempts were made to obtain a good STM image of Au(111)/mica after the adsorption of [2]S-dithiol alone. Out of more

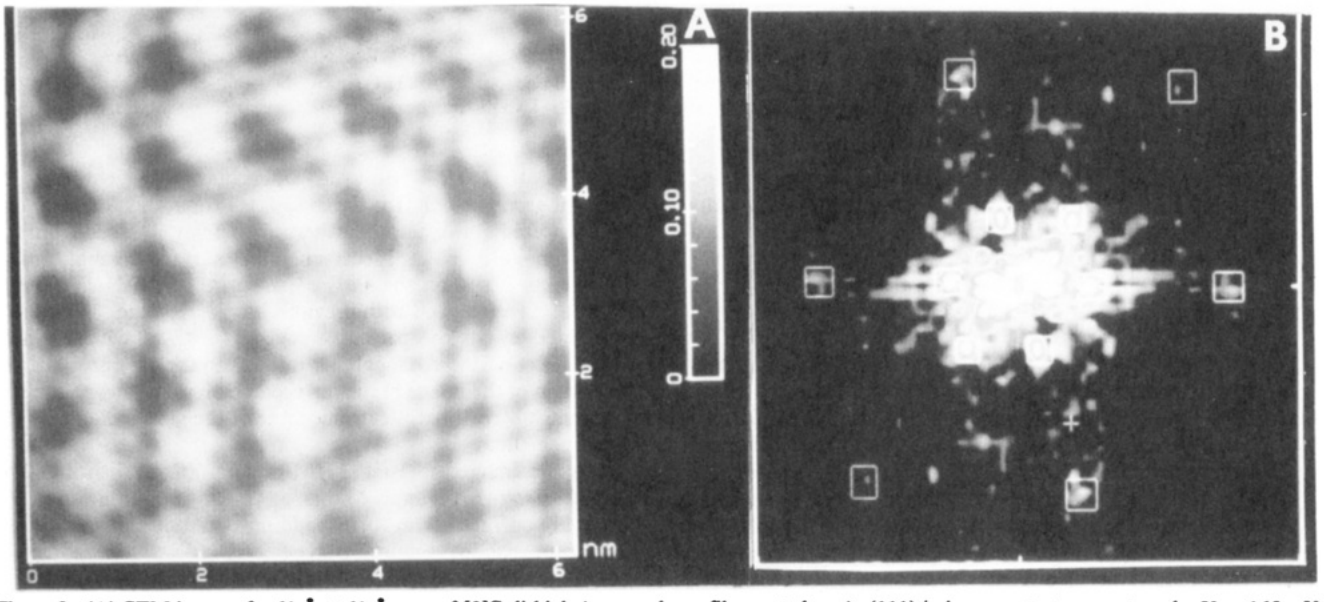

Figure 8. (A) STM image of a 61 Å × 61 Å area of [2]S-dithiol–Ag monolayer film coated on Au(111)/mica: constant-current mode; V_b = 165 mV, I_t = 4.6 nA. (B) Two-dimensional Fourier spectrum of raw data shown in part A. Two distinct hexagonal patterns are clearly observed and used to construct the image shown in part A.

than 15 trials, only one experiment showed atomic-like corrugation (approximately 10 Å spacing, not shown). Otherwise, featureless images were obtained. On the other hand, when Ag was bonded at the ω-thiol group via a metal–S interaction, STM images were easily obtained as demonstrated in Figure 8A. In addition, the periodic features of metal-substituted long chain alkanethiols could be readily identified using STM, as seen in Figures 4 and 5, while the packing structure of unsubstituted alkanethiols (no metal/ligand group) on Au(111) could not. Thus, the metal appears to play an important role in the enhancement of the electron density, even though the metal atom increases the monolayer thickness.

When Figures 6A and 8A are compared, both of them show the same atomic spacings, but the corrugation of the $2(\sqrt{3} \times \sqrt{3})R30°$ structure in Figure 8A is far more distinct and is superimposed on the $(\sqrt{3} \times \sqrt{3})R30°$ structure. Although not as noticeable in Figure 8C, the $(\sqrt{3} \times \sqrt{3})R30°$ structure is still observed (as the outer hexagonal pattern). Thus, the $2(\sqrt{3} \times \sqrt{3})R30°$ structure may represent the image of the staffane moiety and the $(\sqrt{3} \times \sqrt{3})R30°$ structure the modified Au(111) substrate image. On the basis of the images in Figures 6 and 8, and electrochemical data, [2]S-dithiol appears to occupy $2(\sqrt{3} \times \sqrt{3})R30°$ sites on the Au(111) surface.

In conclusion, interpretation of STM images may lead to faulty assignments of adsorbate adlattice structures unless careful consideration of the adsorbate characteristics is taken into account. The image of the substrate atoms and adsorbed species can sometimes be observed simultaneously, but the image can represent a new electronic state of the substrate, not the adsorbate. Although STM is a powerful technique to study surface structure with atomic resolution in air, liquid, or ultrahigh vacuum, caution is needed when interpreting STM images. A complementary technique, such as electrochemistry, can provide helpful information when assigning a structure based on the STM image.

Conclusions

The $(\sqrt{3} \times \sqrt{3})R30°$ superlattice structures of Au(111) were found for the adsorption of different-sized thiol compounds. For the adsorption of 4-ATP, the adlayer structure may be $(\sqrt{3} \times \sqrt{3})R30°$ due to the homogeneous electron density on the surface and the physical size of the molecule. On the other hand, for the bulky compounds such as the [2]S-dithiol–Ag, Ru–[2]S-dithiol, Rub_2b^*, and $(C_5H_5)Fe(C_5H_4CO_2(CH_2)_{16}SH)$, a true $(\sqrt{3} \times \sqrt{3})R30°$ packing cannot be attained and the observed image is caused by substrate gold atoms, i.e., asymmetric electron density on the surface induced by the adsorption of the thiol compounds.

Acknowledgment. We thank Drs. J. Michl, A. Friedl, and Y. Obeng for supplying us with the staffanes and Drs. Y. Obeng and D. Collard for the Rub_2b^* and ferrocenethiol. Our gratitude is expressed to A. Krishnan and Dr. N. Kumar of the Microelectronics and Computation Center for use of evaporation facilities. This work was supported by the Office of Naval Research and the National Science Foundation (CHE-9101924).

References and Notes

(1) Binnig, G.; Rohrer, H.; Gerber, Ch.; Weibel, E. *Phys. Rev. Lett.* **1982**, *49*, 57.

(2) (a) Avouris, P. *J. Phys. Chem.* **1990**, *94*, 2246. (b) Schardt, B. C.; Yau, S.-L.; Rinald, F. *Science* **1989**, *243*, 1050. (c) Magnussen, D. M.; Hotlos, J.; Nichols, R. J.; Kolb, D. M.; Behm, R. *J. Phys. Rev. Lett.* **1990**, *64*, 2929.

(3) (a) Widrig, C. A.; Alves, C. A.; Porter, M. C. *J. Am. Chem. Soc.* **1991**, *113*, 2805. (b) Haussling, L.; Michel, B.; Ringsdorf, H.; Rohrer, H. *Angew. Chem., Int. Ed. Engl.* **1991**, *30*, 569. (c) Kim, Y.-T.; Bard, A. J. *Langmuir* **1992**, *8*, 1096. (d) Smith, D. P. E.; Bryant, A.; Quate, C. F.; Rabe, J. P.; Gerber, Ch.; Swalen, J. D. *Proc. Natl. Acad. Sci. U.S.A.* **1987**, *844*, 969. (e) Smith, D. P. E.; Hober, J. K. H.; Gerber, Ch.; Binnig, G. *Science* **1989**, *245*, 43. (f) Smith, D. P. E.; Hober, J. K. H.; Binnig, G.; Nejoh, H. *Nature* **1990**, *344*, 641. (g) Widrig, C. A.; Chung, C.; Porter, M. D. *J. Electroanal. Chem. Interfacial Electrochem.* **1991**, *310*, 335. (h) Bryant, M. A.; Pemberton, J. E. *J. Am. Chem. Soc.* **1991**, *113*, 8284.

(4) (a) Bryant, A.; Smith, D. P. E.; Quate, C. F. *Appl. Phys. Lett.* **1986**, *48*, 832. (b) Tamanek, D.; Louie, S. G.; Mannin, J.; Abraham, D. W.; Thomson, R. E.; Ganz, E.; Clarke, J. *Phys. Rev. B* **1987**, *35*, 7790. (c) Tamanek, D.; Louis, S. G. *Phys. Rev. B* **1988**, *37*, 8327. (d) Barta, J. P.; Ciraci, S. *J. Vac. Sci. Technol., A* **1988**, *6*, 313.

(5) (a) Mizes, H. A.; Foster, J. S. *Science* **1989**, *244*, 559. (b) Rabe, J. P.; Sand, M.; Batchelder, D. J.; Kalatchev, A. A. *J. Microsc.* **1988**, *152*, 573. (c) Albrecht, T. R.; Mizes, H. A.; Nogami, J.; Park, S.-I.; Quate, C. F. *Appl. Phys. Lett.* **1988**, *52*, 362. (d) Shedd, G. M.; Russel, P. E. *J. Vac. Sci. Technol., A* **1991**, *9*, 1261.

(6) (a) Lyding, J. W.; Hubacek, J. S.; Gammie, G.; Skala, S.; Brockenbrough, R.; Shapley, J. R.; Keyes, M. P. *J. Vac. Sci. Technol. A* **1988**, *6*, 363. (b) Liu, C.-Y.; Chang, H.; Bard, A. J. *Langmuir* **1991**, *7*, 1138. (c) Kuwabara, M.; Clarke, D. R.; Smith, D. A. *Appl. Phys. Lett.* **1990**, *56*, 2396.

(7) (a) Coleman, R. V.; Drake, B.; Hansma, P. K.; Slough, G. *Phys. Rev. Lett.* **1985**, *55*, 394. (b) Wu, X. L.; Lieber, C. M. *Phys. Rev. Lett.* **1990**, *64*, 1150; *J. Am. Chem. Soc.* **1988**, *110*, 5200; *Science* **1989**, *243*, 1703; *Nature* **1988**, *335*, 55. (c) Coleman, R. V.; McNairy, W. W.; Slough, C. G.; Hansma, P. K.; Drake, B. *Surf. Sci.* **1987**, *181*, 112. (d) Coleman, R. V.; Giambattista, B.; Johnson, A.; McNairy, W. W.; Slough, C. G.; Hansma, P. K.; Drake, B. *J. Vac. Sci. Technol., A* **1988**, *6*, 338.

(8) (a) Kaszynski, P.; Michl, J. *J. Am. Chem. Soc.* **1988**, *110*, 5225. (b) Kaszynski, P.; Friedli, A.; Michl, J. *J. Am. Chem. Soc.* **1992**, *114*, 601. (c) Obeng, Y. S.; Laing, M. E.; Friedli, A. C.; Yang, H. C.; Wang, D.; Thulstrup, E. W.; Bard, A. J.; Michl, J. *J. Am. Chem. Soc.*, submitted.

(9) Obeng, Y. S.; Bard, A. J. *Langmuir* **1991**, *7*, 195.

(10) Collard, D.; Fox, M. A. *Langmuir* **1991**, *7*, 1192.

(11) (a) Hallmark, V. M.; Chiang, S.; Rabolt, J. F.; Swalen, J. D.; Wilson, R. J. *Phys. Rev. Lett.* **1987**, *59*, 2879. (b) Chidsey, C. E. D.; Loiacono, D. N.; Sleator, T.; Nakahara, S. *Surf. Sci.* **1988**, *200*, 45.

(12) (a) Nuzzo, R. G.; Allara, D. L. *J. Am. Chem. Soc.* **1983**, *105*, 448. (b) Bain, C. D.; Whitesides, G. M. *J. Am. Chem. Soc.* **1988**, *110*, 5897. (c) Bain, C. D.; Troughton, E. B.; Yao, Y.-T.; Evall, J.; Whitesides, G. M.; Nuzzo, R. G. *J. Am. Chem. Soc.* **1989**, *111*, 321. (d) Sabatani, E.; Rubinstein, I.; Moaz, R; Sagiv, J. *J. Electroanal. Chem.* **1987**, *219*, 365.

(13) Ashcroft, N. H.; Mermin, N. D. *Solid State Physics*; Saunders College: Philadelphia, PA, 1976; p 63.

(14) Chidsey, C. E. D.; Bertozzi, C. R.; Putvinski, T. M.; Mujsce, A. M. *J. Am. Chem. Soc.* **1990**, *112*, 4301.

(15) Murthy, G. S.; Hassenruck, K.; Lynch, V. M.; Michl, J. *J. Am. Chem. Soc.* **1989**, *111*, 7262.

(16) Meyer, T. J. *Acc. Chem. Res.* **1978**, *11*, 94.